CONF-870636--13

SLOSHING AND FLUID-STRUCTURE INTERACTION IN A 400-MWe POOL-TYPE ADVANCED FAST REACTOR

D. C. Ma, J. Gvildys, and Y. W. Chang

CONF-870636--13

DE87 011441

Reactor Analysis and Safety Division
Argonne National Laboratory
9700 South Cass Avenue
Argonne, Illinois 60439 USA

DISCLAIMER

ABSTRACT

This paper describes the seismic analysis of a 400-MWe advanced fast reactor under 0.3 g SSE ground excitation. Two types of analyses are performed -- the sloshing analysis and the fluid-structure interaction analysis. In the sloshing analysis, the sloshing frequency and wave patterns are calculated. The maximum wave height and the sloshing forces exerted on the submerged components and the primary tank are evaluated. In the fluid-structure interaction analysis, the maximum horizontal acceleration for the reactor core and the relative displacement between the reactor core and UIS are examined. The fluid-coupling phenomena between various components are investigated. Seismic stresses at critical areas are examined.

The results obtained from this study are very useful to the design of the advanced reactors. Meanwhile, the computer code FLUSTR-ANL has proved to be a useful analytical tool for assessing the complicated seismic fluid-structure interactions and sloshing in the fast reactor systems.

INTRODUCTION

This paper describes the seismic response of a 400-MWe advanced fast reactor under 0.3-g SSE ground excitation. The objectives of this study are: (1) to determine the sloshing response; (2) to assess the fluid coupling and fluid-structure interaction effects; (3) to demonstrate the capability of the computer code, FLUSTR-ANL (i.e., FLUid-STRucture interaction code, augmented by Argonne National Laboratory for seismic analysis of reactor components); and (4) to obtain useful information for future research needs and code development.

The 400-MWe advanced pool-type fast reactor has a diameter of 39 ft. The reactor plant is designed to be site-independent. This paper describes a transient seismic time-history analysis of the reactor using the FLUSTR-ANL computer code which has been used extensively for prediction of seismically-induced sloshing and fluid-structure interaction responses of reactor systems [1-5]. The ground ZPA varies from 0.2 g to 0.3 g, depending on the site shear-wave velocity (6000 fps to 2000 fps). In this study, the site is assumed to have a shear wave velocity of 2000 fps and the SSE ground ZPA is 0.3 g.

Two types of analyses are performed: the sloshing analysis and the fluid-structure interaction analysis. In both analyses, the excitation motion is a 20-s acceleration time history at the reactor support. The maximum acceleration level is 0.46 g. A 180° sector of the finite element model is developed (half of the reactor). The model contains all the major components of the reactor. All the deck-mounted components (IHX, pump, and UIS) are represented by the beam elements, whereas the reactor vessel and horizontal redan are simulated by the RSDS (Resultant Stress Degenerated Shell) elements [6]. The sodium coolant is simulated by either the displacement-based or pressure-based fluid continuum element. Thin-layer fluid elements are placed at the fluid-structure interfaces to simulate the contact/sliding boundary condition.

Five sections are contained in this paper. The introduction is given in Section I. Section II briefly describes the methodology used in the coupled fluid-structure interaction analysis and the treatment of free surface. Section III gives the description of the reactor, the mathematical model, and the results of the sloshing analysis. In that section, the major concerns of sloshing are described. The sloshing frequencies and wave patterns of the reactor are discussed. The maximum wave height and sloshing forces exerted on the deck-mounted components are evaluated. In Section IV, the seismic analysis of the reactor under horizontal excitation considering fluid-structure interactions is presented. In that section, the lateral vibrational frequencies of the components and the vessel are presented. The core design limits, i.e., the maximum horizontal core acceleration and the relative displacement between the core and UIS are examined to assure that control rods can be properly inserted during scram. The fluid coupling effects on the submerged components are investigated. The seismic stresses at critical areas are evaluated. Finally, the conclusions and recommendations are given in Section V.

COUPLED FLUID-STRUCTURE INTERACTION ANALYSIS

For a coupled fluid-structure interaction analysis, the fluid is represented by fluid finite elements, whereas the reactor vessel and internal components are modeled by shell elements and beam elements. The seismic response of the reactor system is obtained by solving the equations of fluid motion and structural motion simultaneously. The governing equations of fluid dynamics used in the analysis are:

$$\dot{\rho} = -\rho v_{i,i} \tag{1}$$

$$\rho \dot{v}_i = \tau_{ij,j} + b_i \tag{2}$$

$$\tau_{ij} = -p\delta_{i,j} + \mu(v_{i,j} + v_{j,i}) , \tag{3}$$

where ρ is the mass density, b is the body force, p is the pressure, v is the velocity vector of the fluid field, and μ is the dynamic viscosity. The symbol "$\cdot$" denotes the material time derivative, and "," denotes the spatial derivative. The equation of structural motion in matrix form is

$$[m]\{\ddot{d}\} + [c]\{\dot{d}\} + [k]\{d\} = \{P\} , \tag{4}$$

where [m], [c], and [k] are mass, damping, and stiffness matrix, respectively. {d} is the structural displacement vector, and {P} is the fluid pressure acting on structures. At the fluid-structure interface, the fluid velocity normal to the structural surface is required to be equal to the normal component of the structural velocity:

$$v_n = \dot{d}_n , \tag{5}$$

whereas in the tangential direction of the fluid-structure interface, the fluid is allowed to slide freely. The detailed description of FLUSTR-ANL code can be found in Refs. [7,8]. In this paper, only the treatment of free surface is described.

In the analysis, the linear sloshing wave is assumed, and the wave effects are represented by the perturbation pressures P_{fs} acting on the normal direction of the undeformed free-surface and included explicitly in Eq. (4) through the external force vector. The perturbation pressure is obtained from

$$P_{fs} = \rho g d_{fs} , \tag{6}$$

where ρ is the mass density of fluid, g is the gravitational acceleration, and d_{fs} is the free-surface wave height.

SLOSHING ANALYSIS

A pool-type reactor usually contains a large volume of sodium coolant. Under seismic events, the coolant will experience sloshing. The sloshing wave height may easily reach several feet in the large-diameter reactor tanks [5]. If sufficient space is not provided above the free surface to accommodate the sloshing waves, the reactor cover could be damaged by sloshing impact forces and thermal shocks. It may also require an increased height of the thermal liners to protect the IHXs and pumps. Therefore, the sloshing response should be properly considered in the reactor design. This section describes the sloshing analysis of a 400-MWe advanced fast reactor. First, the configuration of the reactor will be briefly described. Then, the sloshing response obtained from the FLUSTR-ANL analysis will be presented.

Description of the Reactor

The isoparametric and elevation views of the reactor model are shown in Figs. 1 and 2, respectively. The major components of the reactor are the reactor vessel, deck structure, deck-mounted components, redan assembly, and reactor core structures. The reactor vessel has a diameter of 39 ft and a length of 47 ft 6 in. The vessel has a 2.5-in-thick cylindrical shell and a 4-in-thick curved bottom head. To simplify the analysis, a conical-shaped bottom head is used. The deck-mounted components include an Upper Internal Structure (UIS) located at the center of the tank and four IHXs, two pumps, and two cold traps placed along the inner perimeter of the reactor tank. The horizontal redan assembly structure separates the coolant into two pools: hot and cold. The sodium coolant in the cold pool, i.e., underneath the redan, is surrounded by the redan, vessel, and shield barrel. It has no free surface and can not participate in the sloshing motion. The sodium coolant above the redan has a free surface and can undergo the sloshing motion. The reactor core is enclosed by a core barrel and the shield barrel. It is supported laterally at the top by the redan assembly structure and vertically at the bottom core support plates which, in turn, are supported by the core support cylinders and the reactor bottom head. The physical dimensions of the components and reactor vessel are given in Table 1.

Mathematical Model

The mathematical model for the sloshing analysis is shown in Fig. 3. Only the hot pool of the coolant above the redan is modeled. The cold coolant below the redan is completely trapped; it does not participate in the sloshing motion and, therefore, is omitted. It is a 180° model representing half of the reactor. The component at the center represents the UIS; the other four off-center components represent two IHXs, one pump, and one cold trap. Thin fluid elements are placed at the fluid-structure interfaces to simulate the contact/sliding boundary condition. The free-surface wave height is treated by a perturbation method as a body force of the fluid, as described above. Only linear sloshing is considered in this study. Since the sloshing frequency and structural frequency are well separated, the components and vessel are assumed to be rigid in the sloshing analysis.

Of particular interest in the sloshing response are the sloshing frequencies, sloshing wave patterns, wave height and sloshing pressures exerted on the components and the vessel. They are often overlooked in the conventional analysis which usually assumed the tank has no internal component [9,10].

Results of the Sloshing Analysis

The input motion at the reactor support is a 20-s long acceleration time history having a maximum acceleration of 0.46 g. A transient time history analysis is carried out to 40 s. The integration time step is 0.1 s.

The results of the sloshing analysis indicates that there are three distinct sloshing modes at frequencies of 0.23 Hz, 0.5 Hz, and 0.9 Hz, respectively. The frequency of 0.23 Hz belongs to the cosθ tangential sloshing mode in which the coolant flows along the tangential direction of the tank. The 0.5-Hz frequency belongs to the radial sloshing mode. In this mode, the coolant sloshes antisymmetrically between the UIS and the vessel along the excitation direction. The frequency of 0.9 Hz belongs to the up-and-down type

wave along the circumferential direction of the tank. The up-and-down sloshing mode occurs mainly in the fluid region bounded by the off-center components and the vessel. The wave patterns of these three modes are shown in Fig. 4, in which H and L indicate the high and low lines of the free surface, and 0 represents a zero line. A typical calculated sloshing wave (at t=7 s) is shown in Fig. 5.

The calculated maximum wave height at various locations on the free surface is shown in Fig. 6. It should be noted that the maximum wave heights shown in Fig. 6 do not occur at the same time. The maximum wave height is 29 in and occurs at IHX-2 (see Fig. 3). The time history of the wave height at that location (node 1668) is shown in Fig. 7, in which the most significant mode is the tangential sloshing mode at a frequency of 0.23 Hz. The maximum wave heights on the UIS and the vessel wall are 17 in and 20 in, respectively (see Fig. 6). They occur at 180° location. The most significant modes at various locations of the free surface are shown in Fig. 8. It indicates that the $\cos^0$ tangential sloshing mode completely dominates the response with the exception of the 0° of the UIS where the radial mode, 0.5 Hz, is still the most significant mode.

In addition to the maximum wave height, the sloshing pressures exerted on the components and the reactor tank are also of importance to the reactor design. There are five layers of fluid elements in the sloshing model (see Fig. 3). The sloshing pressures exerted on the submerged components and the tank wall at layer 1 (top layer), layer 3 (middle layer), and layer 5 (bottom layer) are discussed below. The pressure is calculated at the center of the element.

A typical pressure time history of a fluid element at the top layer is shown in Fig. 9. The sloshing pressure has two components: a convective pressure component which has a longer period of oscillation and an impulsive pressure component which varies synchronously with the input acceleration history. When the input motion stops, the impulsive pressure component vanishes and only the convective pressure component exists. This is clearly indicated in Fig. 9. The convective pressure oscillates at a frequency of 0.23 Hz, which is the frequency of the tangential sloshing motion.

The maximum sloshing pressure at different locations of the three fluid layers are shown in Figs. 10, 11, and 12, respectively. It should be noted that they also do not occur at the same time. The maximum sloshing pressure is 1.3 psi for the reactor tank, 0.50 psi for the UIS, 0.75 psi for the cold trap, 0.66 psi for the pump, 0.92 psi for IHX-1, and 0.96 psi for IHX-2. They all occur at the bottom fluid layer.

The pressure time history and FFT plot at fluid element 320 on the bottom of IHX-2, where the maximum sloshing motion occurs, are shown in Fig. 13. The FFT shows that the pressure time history has two distinct frequencies: one is 0.9 Hz and the other is 0.23 Hz. The contribution of impulsive pressures which have higher frequencies can also be observed. Figures 14, 15, and 16 summarize the most dominant frequency of the sloshing pressures at various locations for the three fluid layers. On layer 1, the most important mode is the $\cos\theta$ tangential sloshing which has a frequency of 0.23 Hz. However, the sloshing mode with a frequency of 0.9 Hz can be found at certain locations of the components. As the fluid depth increases from layer 1 to layer 5, the intensity of impulsive pressure increases. This can be seen in Figs. 15 and 16, where the 0.23-Hz sloshing frequency in certain areas is replaced by impulsive pressure frequencies of 1.7 Hz, 1.9 Hz, and 2.9 Hz and no longer is the dominant frequency. It is interesting to note that the magnitude of the 0.9-Hz sloshing mode also increases with the fluid depth. This mode has a pronounced effect on the tank and the off-center components. As a result, the total pressures at the bottom of the tank are larger than those near the surface.

The sloshing forces acting on the components and the tank wall are examined next. On the off-center components, there are two types of sloshing modes: one is the tangential sloshing mode which has a frequency of 0.23 Hz; the other is the up-and-down type of mode having a frequency of 0.9 Hz. It is reasonable to assume that at certain instances, the pressure acting on the component has a $\cos\theta$ distribution, as shown in Fig. 17. In other words, one side of the component is subjected to compressive loads while the other side is subjected to tensile loads. It is the worst loading case that a component can be subjected to under seismic sloshing. As a conservative estimate, the maximum sloshing pressure of 0.96 psi acting on IHX-2 is used to calculate the sloshing force acting on the components under the most unfavorable condition. It is further assumed that the sloshing pressure is uniformly distributed along the submerged length of the component. The resultant force, f, acting on the unit length of the component (see Fig. 18) is

$$f = \int_0^{2\pi} P \cdot \cos^2\theta \, r\,d\theta \qquad (7)$$

or

$$f = \pi p r \,, \qquad (8)$$

where P is the maximum sloshing pressure and r is the radius of the component. The total sloshing force, F, acting on the component is

$$F = f \cdot \ell \,, \qquad (9)$$

where ℓ is the submerged length of the components measured from the surface of the sloshing wave.

For the case studied, the IHX-2 has a submerged length of 14 ft and a length of 10 ft above the free surface. The maximum sloshing wave height for IHX-2 is 29 in. The diameter of IHX-2 is 6 ft-10 in. If the wall thickness of the IHX-2 is assumed to be 1 in, the maximum bending stress at the base support is only 1 ksi.

The sloshing force exerted on the tank wall is also quite small. Generally speaking, the seismic stresses due to sloshing is small compared to other types of stresses.

SEISMIC FLUID-STRUCTURE INTERACTION ANALYSIS

Mathematical Model

This section describes the seismic fluid-structure interaction analysis of the reactor. Only the horizontal ground excitation is considered in the analysis. The mathematical model is shown in Figs. 1 and 2. The model includes: the reactor vessel, UIS, cold trap, one pump, two IHXs, redan assembly, and core structures. The reactor vessel and redan plate are represented by the RSDS (Resultant Stress Degenerated Shell) elements. The components, thermal liner, skirt extension of the shield barrel, and core structures (including shield barrel and core-support cylinders) are represented by the beam elements. Because of the complexity of the IHX, an equivalent beam with a fundamental frequency of 3.5 Hz (in-air frequency of IHX) is used. The beams representing the IHXs and UIS are suspended from the deck. The beams representing the

shroud of the pump and cold trap are supported on the redan plate. The beam representing the core structures is laterally supported by the redan at the top of the core and by the reactor bottom head at the bottom of the core.

The model consists of 3290 nodal points, 351 displacement-based fluid elements, 1331 pressure-based fluid elements, 463 RSDS shell elements, and 57 beam elements. It is a very detailed reactor model. The horizontal input motion is the same acceleration time history used in the sloshing analysis. It has a duration of 20 s and a maximum acceleration of 0.46 g, which occurs at t = 8.1 s. Since the maximum acceleration occurs within the first 10 s of ground motion, the time history analysis is carried only to 12 s. The integration time step is 0.005 s. Three percent (3%) of the structural damping is used.

Under horizontal seismic excitation, the maximum horizontal acceleration of the reactor core and the relative lateral displacement of the core and UIS are of particular importance. The design limits of the reactor core under SSE conditions are 3.5 g for horizontal core acceleration and 2.2 in for relative displacement between the top of the core and the bottom of the UIS. In addition to the core response, the fluid coupling effects between components and seismic stresses at critical areas are also important concerns.

Results of Seismic Fluid-structure Interaction Analysis

The analysis indicates that there are three significant lateral modes. The first is the IHX lateral vibrational mode which has a frequency of 5.67 Hz. The second is the vessel-core-redan mode which has a frequency of 9 Hz. The third is the UIS lateral mode which has a frequency of 12.5 Hz.

The displacement time history and FFT at the bottom of the UIS and top of the core are shown in Figs. 19 and 20, respectively. They indicate that the maximum displacement of the UIS and the core is 0.047 in and 0.070 in, respectively. They occur at the same time, i.e., t = 8.15 s. The sum of the absolute value of the two displacements is only 0.117 in, which is well below the design limit of 2.2 in. The displacement time history and FFT of the UIS (see Fig. 19) indicate that the UIS has a vibrational frequency of 12.5 Hz. Also shown in Fig. 19 are the other significant modes. One has a frequency of 5.67 Hz and the other has a frequency of 0.23 Hz. The 5.67-Hz frequency is caused by the vibration of the IHX which is transmitted to the UIS by the fluid coupling effect. The 0.23-Hz frequency is the sloshing frequency transmitted to the UIS by the lateral sloshing force. The other peaks observed in the FFT plot belong to the input motion. The influence of the IHX on the core response can also be found in the FFT of the core (see Fig. 20).

The displacement response and FFT at the bottom of IHX-1 and IHX-2 are shown in Figs. 21 and 22, respectively. The maximum lateral displacements of IHX-1 and IHX-2 are 0.32 in and 0.36 in, respectively. Both IHXs vibrate at a frequency of 5.67 Hz. It is noted that the in-air frequency of the IHX is 3.5 Hz. The increase in frequency is due to the influence of the vessel vibration on the IHXs. This influence can be seen from the plots of FFT of the IHX (see Figs. 21 and 22).

The displacement response and FFT at the bottom of the vessel, the top of the pump well, and the top of the cold trap are shown in Figs. 23, 24, and 25, respectively. Basically, the vessel, core, pump well, and cold trap move in unison, having a frequency of 9 Hz. The effects of the IHX vibration of 5.67 Hz frequency are clearly shown in Figs. 23, 24, and 25. The maximum lateral displacement and the first (f_1) and second (f_2) dominant frequencies at various locations are summarized in Table 2. The second dominant frequency, f_2, represents the fluid coupling effects. The maximum acceleration of the core, a, can be obtained from

$$a = d \cdot (2\pi f)^2 , \qquad (10)$$

in which d and f are the maximum displacement and the frequency of the core, respectively. For the case studied here, d = 0.086 in and f = 9 Hz, the maximum acceleration at the core is 0.7 g. It is much smaller than the allowable core acceleration under SSE conditions, i.e., 3.5 g. In general, the seismic stresses are small. The maximum bending stress is only 2.3 ksi at the base of the UIS.

CONCLUSIONS AND RECOMMENDATIONS

Seismic analysis has been performed for a pool-type advanced fast reactor with a diameter of 39 ft. The analysis considers the sloshing and fluid-structure interactions under horizontal seismic excitation. Much valuable information has been obtained. It can be used as a design reference for future reactors. The conclusions and recommendations drawn from this study are summarized below.

1. The most significant mode of the reactor is the core-vessel lateral vibration mode which has a frequency of 9 Hz and which is considerably higher than that of a large-diameter reactor. The other two significant modes are the IHX lateral vibration mode, 5.6 Hz, and the UIS lateral vibration mode, 12.5 Hz. Because of high frequencies, the overall seismic response of the reactor is small. The maximum horizontal acceleration of the reactor core is 0.7 g, and the maximum relative displacement of the UIS and reactor core, i.e., the displacement of the top of the reactor core with respect to the bottom of the UIS, is only 0.117 in. They are considerably lower than the core design limits. The maximum core horizontal acceleration limit is 3.5 g, whereas the maximum displacement limit between the UIS and the reactor core is 2.2 in. The seismic stresses are also small.

2. Strong interaction (fluid coupling) exists between the IHXs and the vessel. As a result, the IHX frequency increases to 5.6 Hz. Note that the in-air IHX frequency is only 3.5 Hz. On the other hand, the vessel-core response has also been strongly influenced by the vibration of the IHXs. This is also true for the UIS. It is strongly influenced by the vibration of the IHX.

3. In the sloshing analysis, three sloshing modes have been identified. They are the cosθ tangential sloshing mode which has a frequency of 0.23 Hz, the radial sloshing mode which has a frequency of 0.5 Hz, and the up-and-down tangential sloshing mode which has a frequency of 0.9 Hz. The sloshing response is dominated by the cosθ tangential sloshing mode in which the sodium coolant flows along the tangential direction of the tank. The radial sloshing mode is confined in the fluid region between the UIS and the vessel along the excitation direction. The up-and-down tangential sloshing mode occurs mainly in the fluid region bounded by the off-center components and the vessel. This mode has a pronounced effect on the sloshing pressure as the fluid depth increases from the surface.

4. The maximum sloshing wave height is 29 in, which occurs at the IHX-2 location. The maximum sloshing pressure exerted on the submerged components is less than 1 psi. The bending stress at the component base due to the sloshing pressure is not significant.

ACKNOWLEDGEMENTS

The authors wish to express their sincere gratitude to Mr. R. W. Seidensticker for his encouragement and support during this study. This work was performed in the Engineering Mechanics Program of the Reactor Analysis ans Safety Division of Argonne National Laboratory under the auspices of the U.S. Department of Energy, Office of Technology Support Programs, under contract W-31-109-ENG-38.

REFERENCES

1. Ma, D. C., Gvildys, J., Chang, Y. W., and Seidensticker, R. W., "Seismically Induced Sloshing Phenomena in LMFBR Reactor Tanks," Advances in Containment Design and Analysis, Bd. Vol. C00214, ASME/ANS Nuclear Engineering Conference, Portland, OR, July 1982.

2. Ma, D. C., Liu, W. K., Gvildys, J., and Chang, Y. W., "Seismic Behavior of Liquid-Filled Shells, "Nuclear Engineering and Design, 70, 1982.

3. Liu, W. K. and Ma, D. C., "Coupling Effect Between Liquid Sloshing and Flexible Fluid-Filled Systems," Nuclear Engineering and Design, 72, pp. 345-357, 1982.

4. Ma, D. C., Gvildys, J., and Chang, Y. W., "Seismic Fluid-Structure Interaction of a Large Breeder Reactor," Seismic Effects of PVP Components (ASME special publication of 1984 PV&P Conference, edited by V. N. Shah and D. C. Ma).

5. Ma, D. C. and Chang, Y. W., "Analysis of Seismic Sloshing of Reactor Tanks Considering Submerged Components and Seismic Isolation," Proceedings of the 1985 PV&P Conference, New Orleans, LA, June 23-26, 1985, Fluid-Structure Dynamics, PVP - Vol. 98-7, pp. 139-149, edited by D. C. Ma and F. Moody.

6. Liu, W. K., Law, E., Lam, D., and Belytschko, T., "Resultant Stress Degenerated Shell Elements," Computer Methods in Applied Mechanics and Engineering, Vol. 55, 1986, pp. 259-300.

7. Chang, Y. W., Ma, D. C., Gvildys, J., and Liu, W. K., "Seismic Analysis of LMR Reactor Tanks," to be appeared in Journal of Nuclear Engineering and Design.

8. Liu, W. K. and Ma, D. C., "Computer Implementation Aspects for Fluid-Structure Interaction Problems," Computer Methods in Applied Mechanics and Engineering, 31, (1982), pp. 129-148.

9. "Pool-Type LMFBR Plant 1000-MWe Phase A-Extension-1 Design," EPRI NP-882, Vol. 4, September 1978.

10. "Pool-Type LMRBR Plant 1000-MWe Phase A-Extension-2 Design," EPRI NP-1014, Vol. 7, June 1979.

Table 1. Physical Dimensions of the Components and the Vessel

	Radius (in)	Thickness (in)
UIS	40	1
Cold Trap	29	0.75
Pump Well	40	2.5
IHX	41	*
Shield Barrel	90	2
Shield Barrel Skirt	92	1
Redan	--	3
Vessel - Cylinder	220	2.5
Vessel - Bottom Head	--	4

*Equivalent Beam

Table 2. Maximum Lateral Displacement and Dominant Frequencies at Various Locations

	Maximum Disp. (in)	f_1 (Hz)	f_2 (Hz)
Bottom of UIS	0.047	12.5	5.67
Top of Core	0.070	9.0	5.67
Bottom of Core	0.086	9.0	5.67
Bottom of IHX-1	0.32	5.67	9.0
Bottom of IHX-2	0.36	5.67	9.0
Top of Pump Well	0.078	9.0	5.67
Top of Cold Trap	0.083	9.0	5.67
Redan	0.068*	9.0	5.67

*Maximum displacement at base of pump well and cold trap

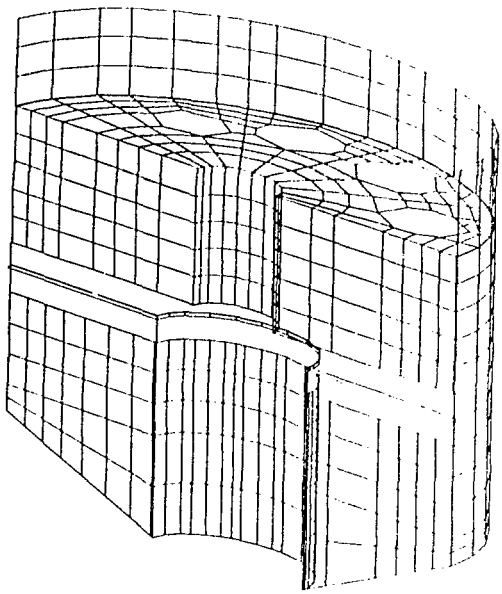

Fig. 1. Isoparametric View of Reactor Mathematical Model

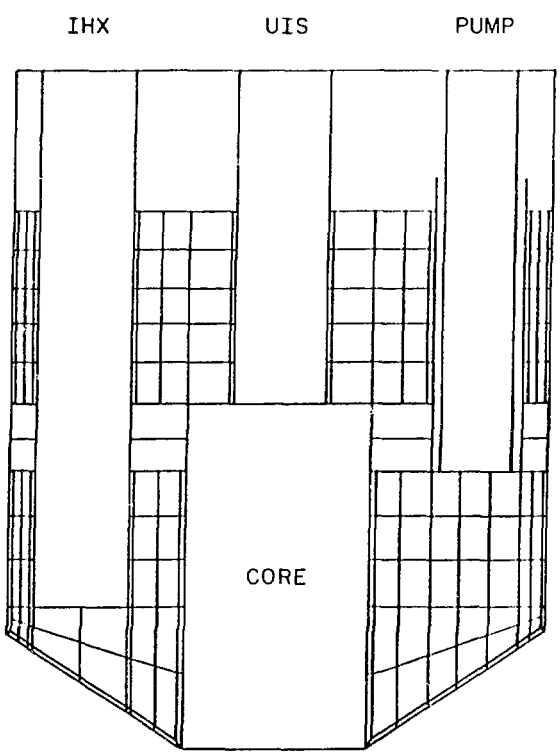

Fig. 2. Elevation View of Reactor Mathematical Model

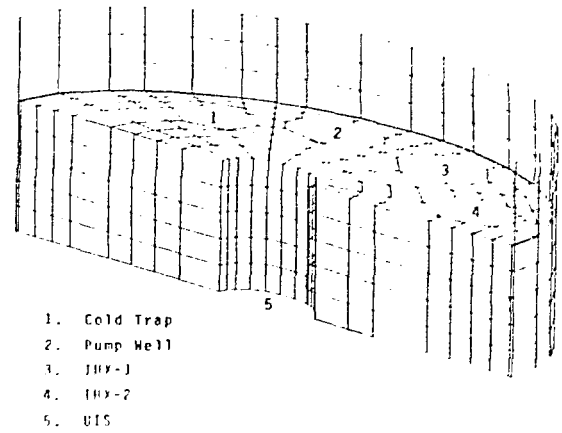

Fig. 3. Mathematical Model for Sloshing Analysis

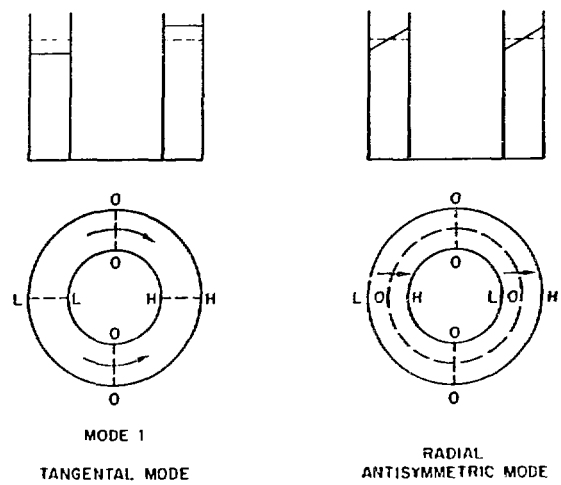

Fig. 4. Sloshing Wave Patterns

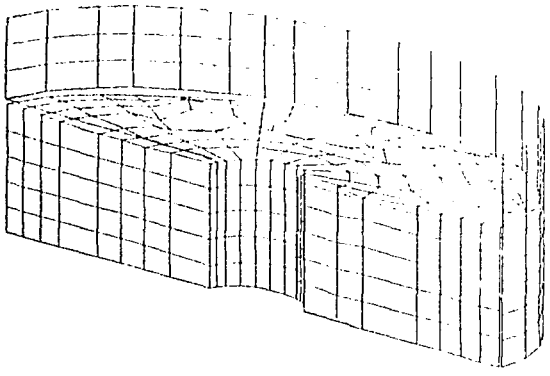

Fig. 5. Sloshing Wave at t = 7 s

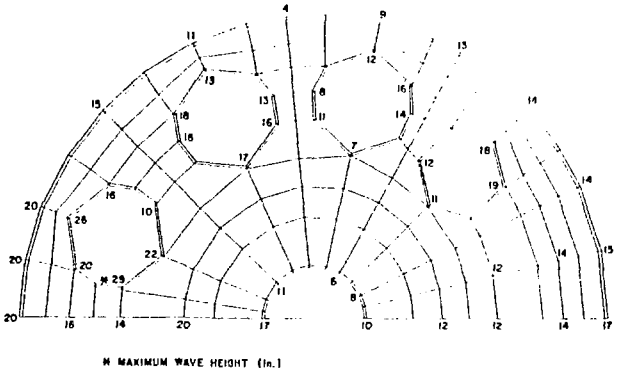

Fig. 6. Maximum Wave Height (in) at Free Surface

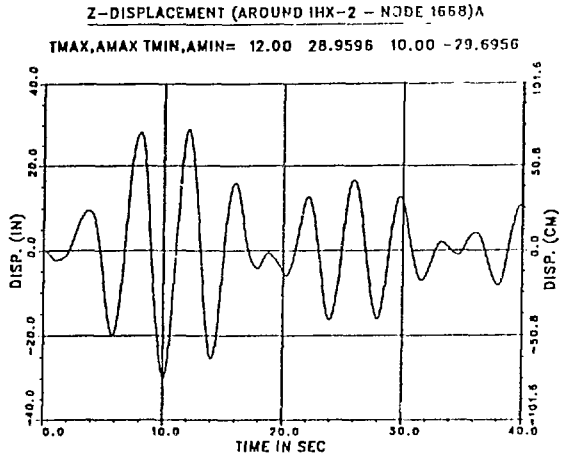

Fig. 7. Sloshing Wave Height

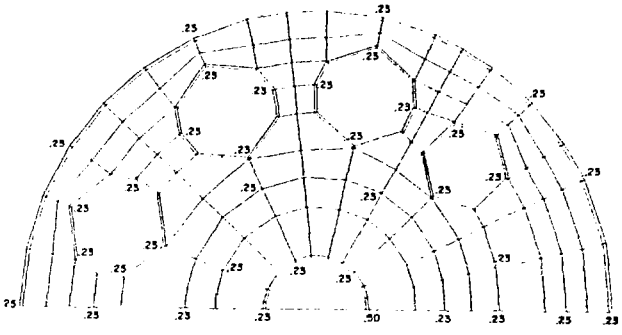

Fig. 8. *Frequency of the Dominant Modes at Different Locations on the Free Surface*

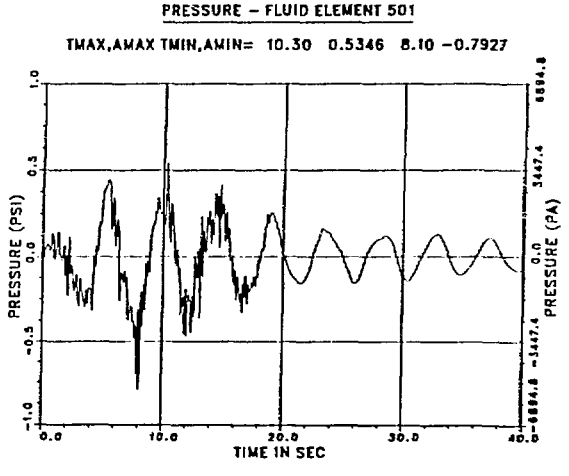

Fig. 9. Pressure of Fluid Element 501 at Free Surface

Fig. 10. Magnitude of Maximum Sloshing Pressures (psi) on Layer 1

Fig. 11. Magnitude of Maximum Sloshing Pressures (psi) on Layer 3

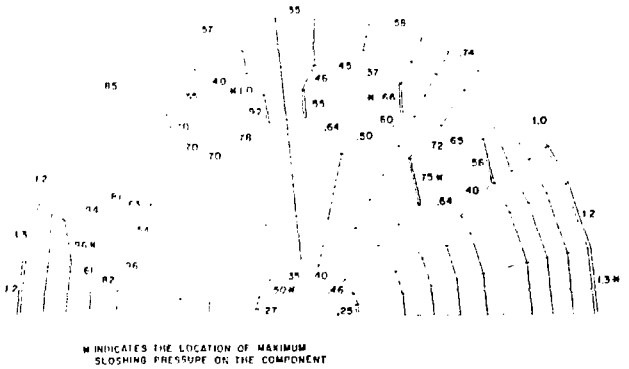

Fig. 12. Magnitude of Maximum Sloshing Pressure (psi) on Layer 5

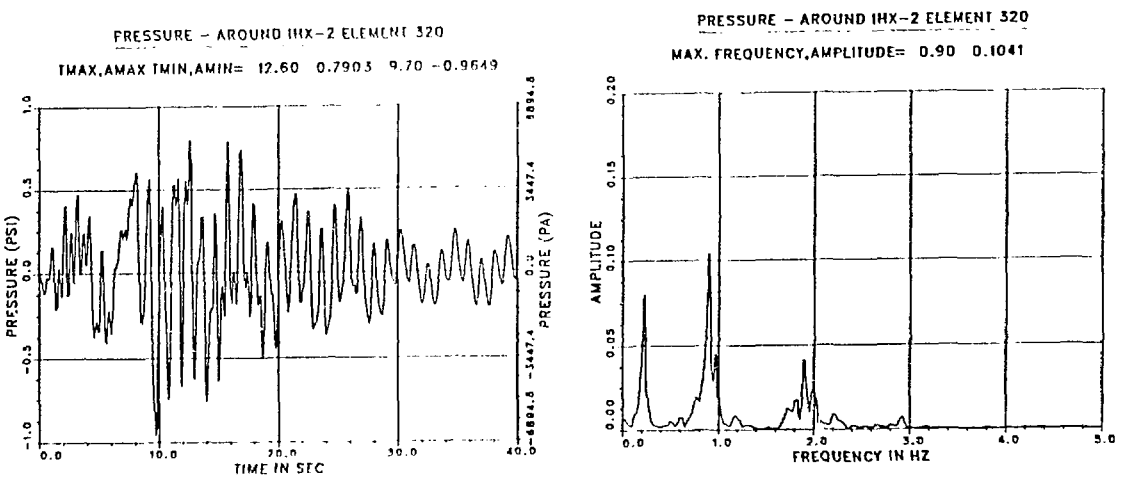

Fig. 13. Pressure Time History and FFT of Fluid Element 320

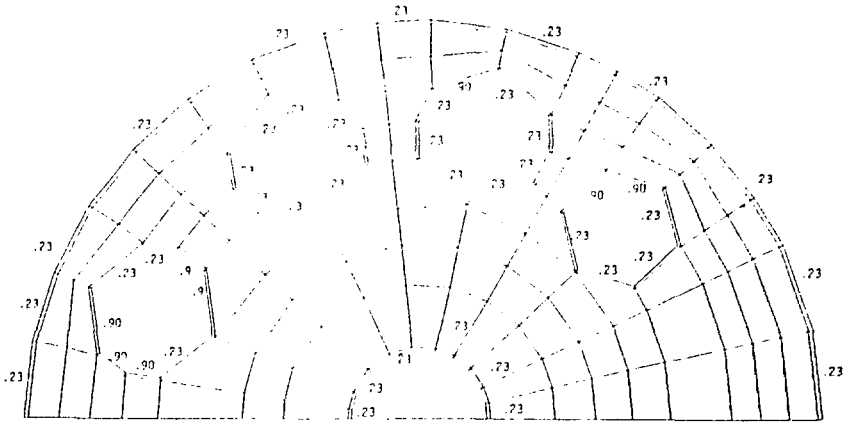

Fig. 14. Frequency of Dominant Modes of Sloshing Pressure on Layer 1

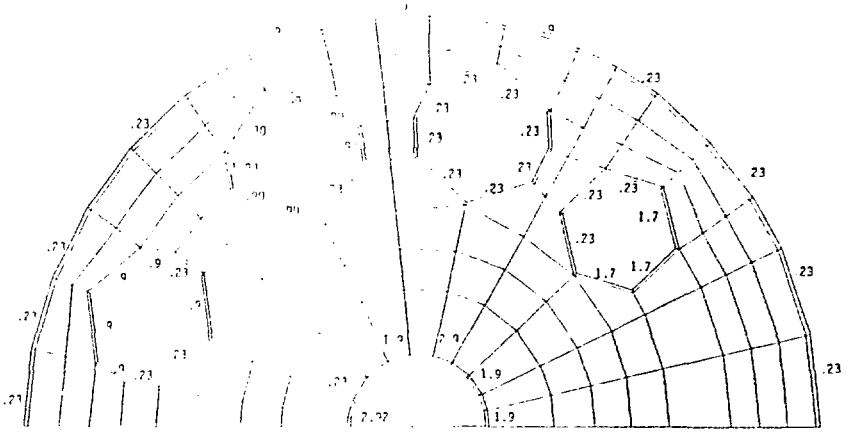

Fig. 15. Frequency of Dominant Modes of Sloshing Pressure on Layer 3

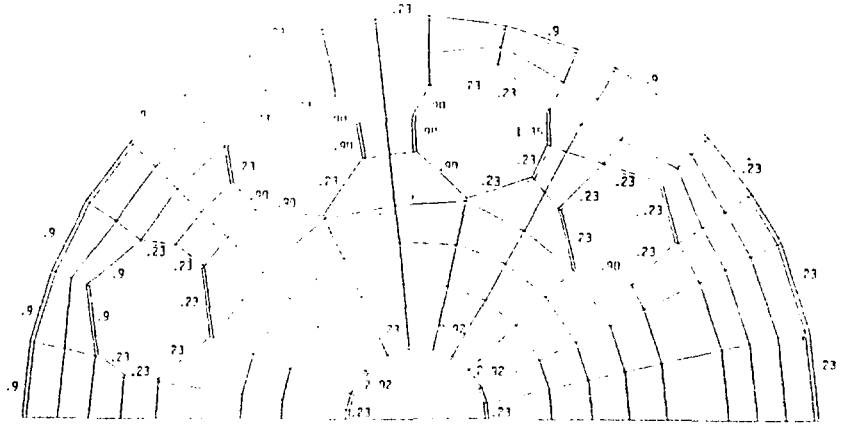

Fig. 16. Frequency of Dominant Modes of Sloshing Pressure on Layer 5

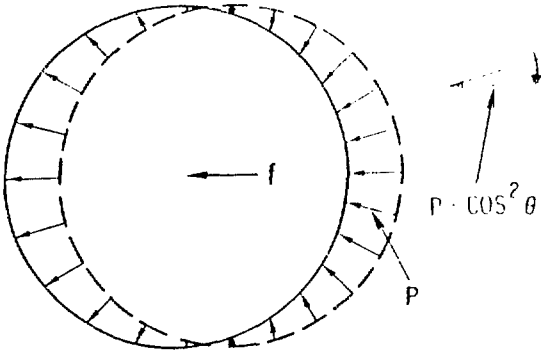

Fig. 17. Distribution of Sloshing Pressures on a Component

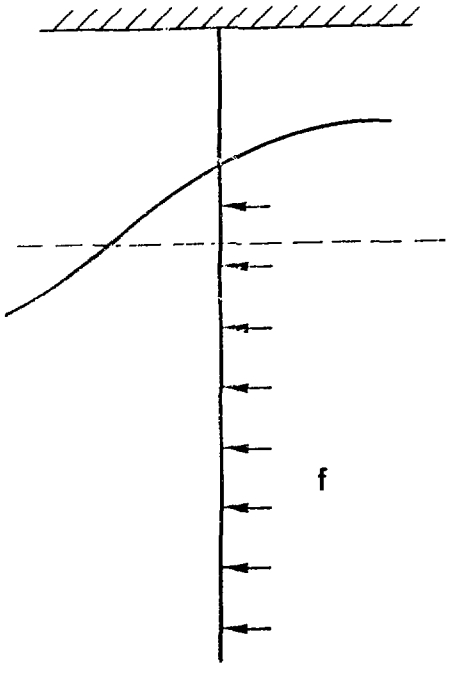

Fig. 18. Sloshing Force on a Submerged Component

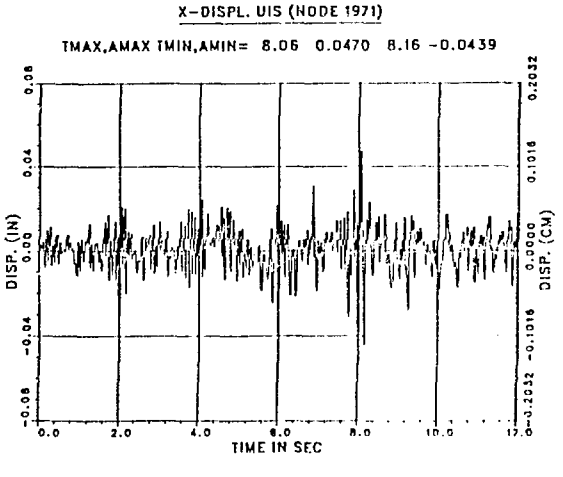

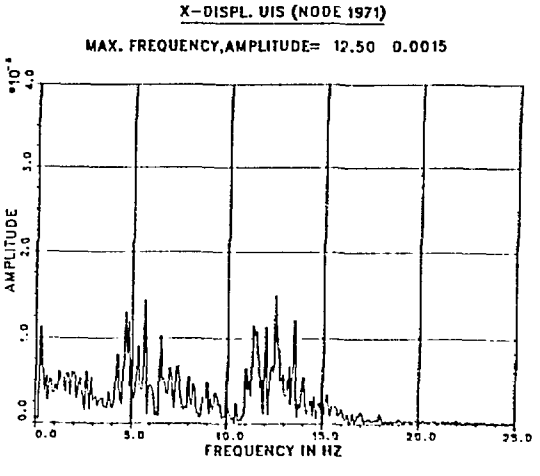

Fig. 19. Horizontal Displacement Time History and FFT at the Bottom of the UIS

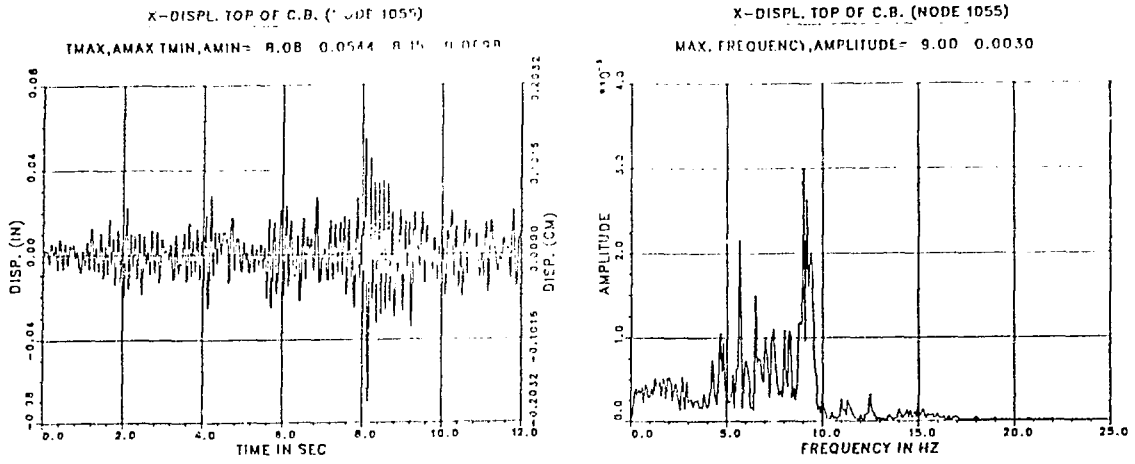

Fig. 20. Displacement Time History and FFT at the Top of the Reactor Core

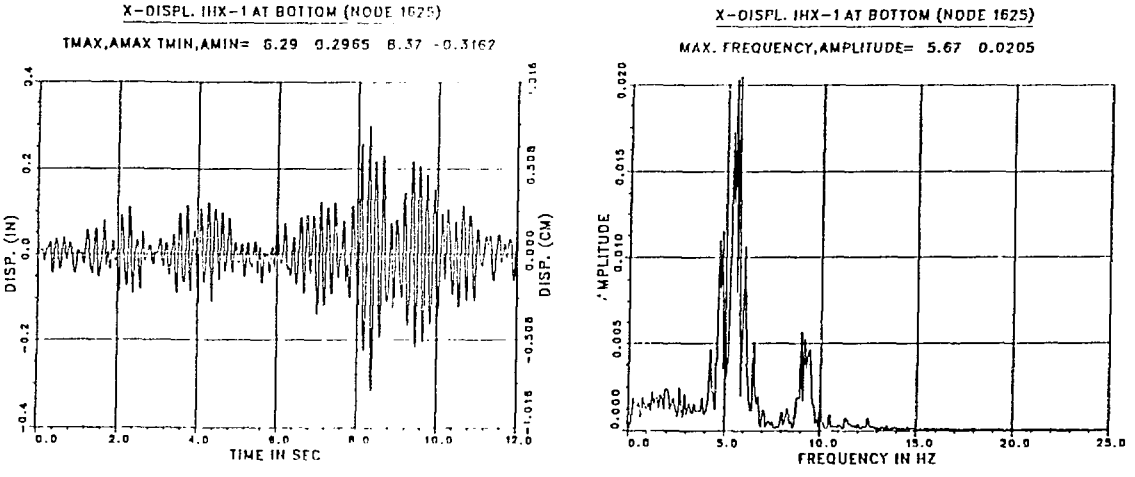

Fig. 21. Displacement Time History and FFT at the Bottom of IHX-1

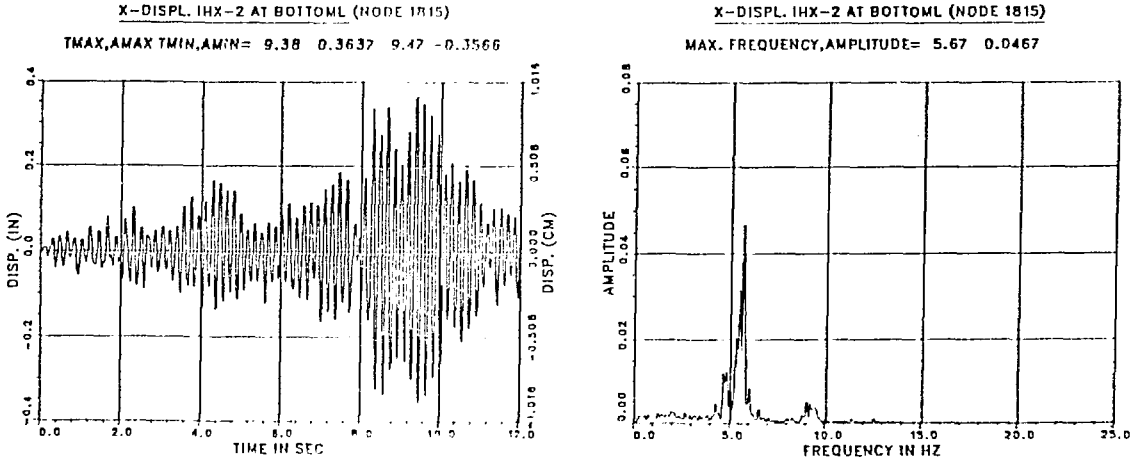

Fig. 22. Displacement Time History and FFT at the Bottom of IHX-2

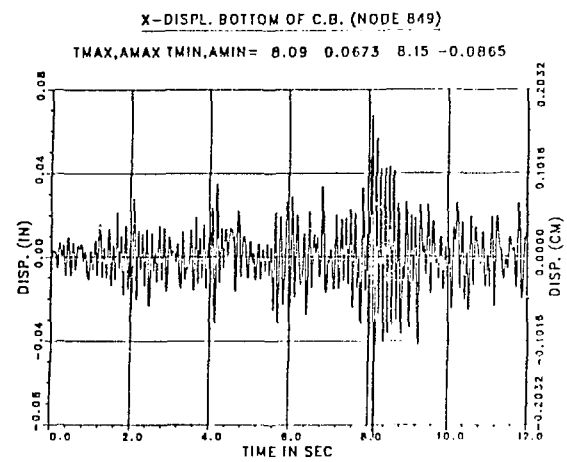

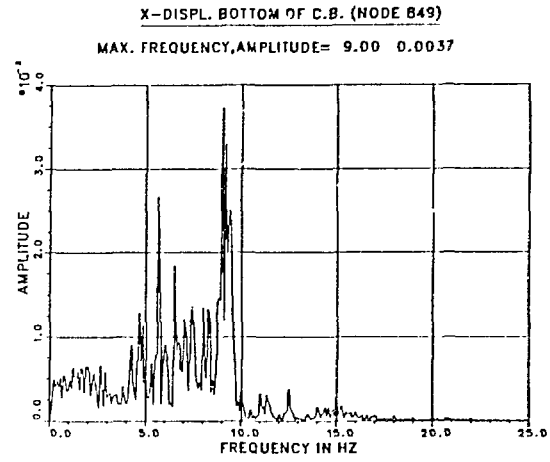

Fig. 23. Displacement Time History and FFT at the Bottom of the Vessel

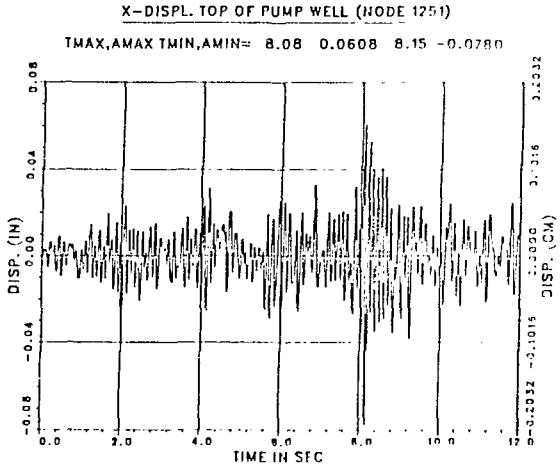

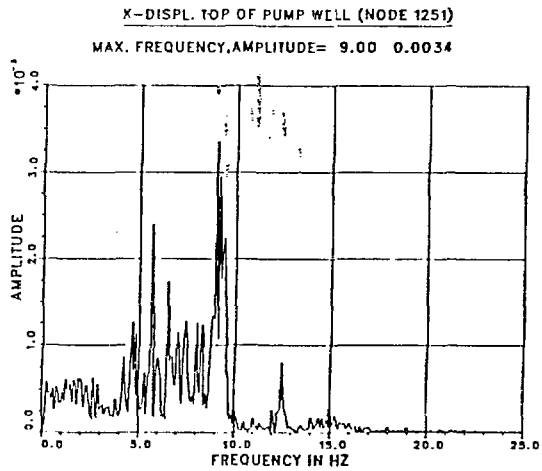

Fig. 24. Displacement Time History and FFT at the Top of the Pump Well

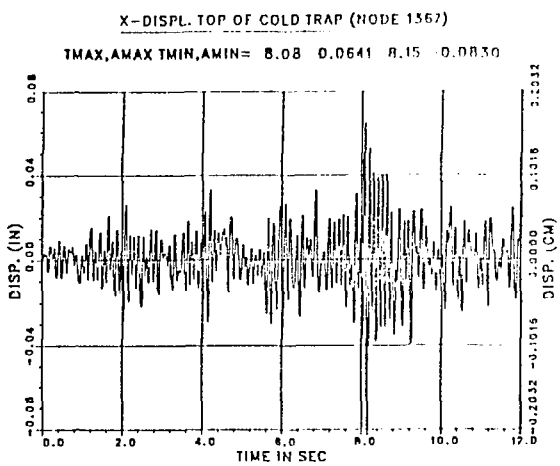

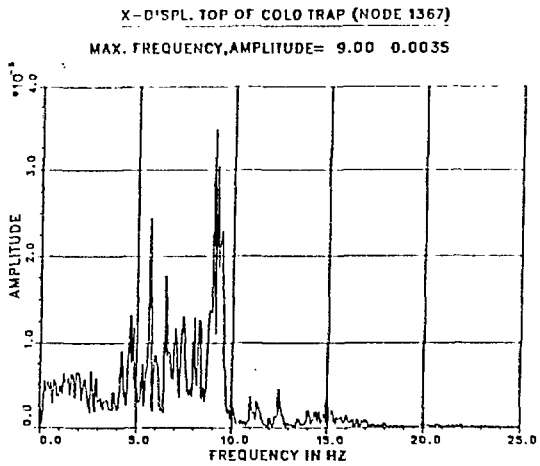

Fig. 25. Displacement Time History and FFT at the Top of the Cold Trap